Observation of the topological surface state in the nonsymmorphic topological insulator KHgSb

A. J. Liang,[1] J. Jiang,[1,2,3] M. X. Wang,[1] Y. Sun,[4] N. Kumar,[4] C. Shekhar,[4] C. Chen,[5] H. Peng,[5] C. W. Wang,[6] X. Xu,[2,7] H. F. Yang,[1,6] S. T. Cui,[1] G. H. Hong,[1] Y.-Y. Xia,[1,4] S.-K. Mo,[2] Q. Gao,[8] X. J. Zhou,[8,9] L. X. Yang,[7] C. Felser,[4] B. H. Yan,[10] Z. K. Liu,[1,*] and Y. L. Chen[1,5,7,11,†]

[1]*School of Physical Science and Technology, ShanghaiTech University, Shanghai 201210, People's Republic of China*
[2]*Advanced Light Source, Lawrence Berkeley National Laboratory, Berkeley, California 94720, USA*
[3]*Pohang Accelerator Laboratory, POSTECH, Pohang 790-784, Korea*
[4]*Max Planck Institute for Chemical Physics of Solids, D-01187 Dresden, Germany*
[5]*Department of Physics, University of Oxford, Oxford OX1 3PU, United Kingdom*
[6]*State Key Laboratory of Functional Materials for Informatics, SIMIT, Chinese Academy of Sciences, Shanghai 200050, People's Republic of China*
[7]*State Key Laboratory of Low Dimensional Quantum Physics, Department of Physics and Collaborative Innovation Center of Quantum Matter, Tsinghua University, Beijing 100084, People's Republic of China*
[8]*Beijing National Laboratory for Condensed Matter Physics, Institute of Physics, Chinese Academy of Sciences, Beijing 100190, People's Republic of China*
[9]*Collaborative Innovation Center of Quantum Matter, Beijing 100190, People's Republic of China*
[10]*Department of Condensed Matter Physics, Weizmann Institute of Science, Rehovot 7610001, Israel*
[11]*Hefei Science Center, CAS and SCGY, University of Science and Technology of China, Hefei 230026, People's Republic of China*

(Received 1 June 2017; published 25 October 2017)

Topological insulators represent unusual topological quantum states, typically with gapped bulk band structure but gapless surface Dirac fermions protected by time-reversal symmetry. Recently, a distinct kind of topological insulator resulting from nonsymmorphic crystalline symmetry was proposed in the KHgX (X = As, Sb, Bi) compounds. Unlike regular topological crystalline insulators, the nonsymmorphic glide-reflection symmetry in KHgX guarantees the appearance of an exotic surface fermion with hourglass shape dispersion (where two pairs of branches switch their partners) residing on its (010) side surface, contrasting to the usual two-dimensional Dirac fermion form. Here, by using high-resolution angle-resolved photoemission spectroscopy, we systematically investigate the electronic structures of KHgSb on both (001) and (010) surfaces and reveal the unique in-gap surface states on the (010) surface with delicate dispersion consistent with the "hourglass Fermion" recently proposed. Our experiment strongly supports that KHgSb is a nonsymmorphic topological crystalline insulator with hourglass fermions, which serves as an important step to the discovery of unique topological quantum materials and exotic fermions protected by nonsymmorphic crystalline symmetry.

DOI: 10.1103/PhysRevB.96.165143

The investigation on topological quantum states, including topological insulators [1–8], topological crystalline insulators [9–14], and topological semimetals [15–32], has become one of the most intensively studied topics in condensed matter physics. These topological quantum states possess unique fermions (such as two-dimensional (2D) and three-dimensional (3D) Dirac fermions [1–23], Weyl fermions [24–42], and Majorana fermions [43,44]) which can host many fascinating physical phenomena (such as the QSH effect [4,5], QAH effect [45,46], and XMR [47–57]). Remarkably, as these fermions and phenomena are protected by symmetries (e.g., time-reversal symmetry and space-group symmetries), they are robust against perturbations.

Recently, the nonsymmorphic-symmetry-protected topological quantum states, including topological insulators and semimetals, were under intensive research [58–68]. Among them, KHgX (X = As, Sb, Bi) compounds were proposed as the first family of nonsymmorphic topological insulator [65,66]. According to the *ab initio* calculations [65], KHgX are insulating in the bulk but possess robust gapless surface states [see Fig. 1(a)], forming the unique "hourglass Fermions" on the (010) surface. The surface fermion contains four-branch (quadruplet) dispersions [Fig. 1(b)] and unbreakable zigzag chainlike patterns [65]. These surface states can also be understood as two copies of surface states of weak topological insulators [69]. The nonsymmorphic glide-reflection symmetry protects these two copies from annihilating with each other inside the mirror plane. In order to visualize the intriguing hourglass fermion surface states and confirm the nonsymmorphic topological insulator nature of KHgX, ARPES is the natural experimental tool. The theoretical proposal of an hourglass fermion was followed by a recent ARPES study [67]. However, the identification of the quadruplet surface states was not completely clear as they coexist with the bulk continuum [67].

In this work, we report a comprehensive ARPES study on the electronic structures of KHgSb on both (001) and (010) surfaces. On the (001) surface, we observed insulating bulk states over the whole Brillouin zone with an indirect band gap of ~200 meV without any signature of in-gap surface states. Remarkably, on the (010) surface, we observed clear in-gap surface states with dispersions consistent with the hourglass configuration, as proposed in a recent theoretical work [65]. The broad agreement between the experimental

*liuzhk@shanghaitech.edu.cn
†yulin.chen@physics.ox.ac.uk

results and the *ab initio* calculations strongly supports that KHgSb is a nonsymmorphic topological crystalline insulator with hourglass fermions, which serves as an important step to the discovery of unique topological quantum materials and exotic fermions protected by the nonsymmorphic crystalline symmetry.

I. BASIC INFORMATION ON KHgSb

High-quality KHgSb crystals were synthesized by the flux method (see Appendix for details). The crystal structure of KHgSb is shown in Fig. 1(c) with space group $P6_3/mmc$ and lattice constants $a = b = 4.78$ Å, $c = 10.225$ Å. The in-plane Hg and Sb atoms show strong bonding, forming in-plane honeycomb lattices. The off-plane K atoms sit above the center of each honeycomb, sandwiched loosely by the two adjacent layers and serve as their inversion center. The natural cleavage surface is along the (001) surface and (010) surface (parallel to the diagonal of the in-plane honeycomb; it preserves the glide-reflection symmetry). The bulk Brillouin zone (BZ) and the surface BZs of both (001) and (010) surfaces are shown in Fig. 1(d). Figures 1(e) and 1(f) illustrate the broad constant energy contours (CECs) at Fermi level across multiple BZs on the (001) and (010) surfaces, respectively, confirming the cleaved surfaces with correct lattice parameters [the momentum directions of $k_x/k_y/k_z$ are defined to be parallel to $\tilde{\Gamma}-\tilde{X}$, $\bar{\Gamma}-\bar{K}$, and $\tilde{\Gamma}-\tilde{Z}$, respectively; see Fig. 1(d)]. The core level photoemission spectra [Fig. 1(g)] show sharp characteristic Sb_{4d}, K_{3p}, and Hg_{5d} levels.

II. ELECTRONIC STRUCTURES ON THE (001) SURFACE

We first focus on the electronic structures on the (001) surface. According to the band structure calculation [65], KHgSb is a fully gapped nonsymmorphic crystalline topological insulator without surface states residing on the (001) surface. From the 3D plot of the electronic structure [Fig. 2(a)] and the stacked plot of CECs [Fig. 2(b)], one clearly sees that the bands near $\bar{\Gamma}$ are holelike. The sixfold rotational symmetry of the CECs further confirms the (001) surface cleavage. The diminished intensity of the CEC at Fermi level [Figs. 2(a)–2(c)] and the band dispersions [Fig. 2(f)] near Fermi level indicate that the Fermi energy resides just above the top of the valence band. In addition, both the CECs [Fig. 2(c)]

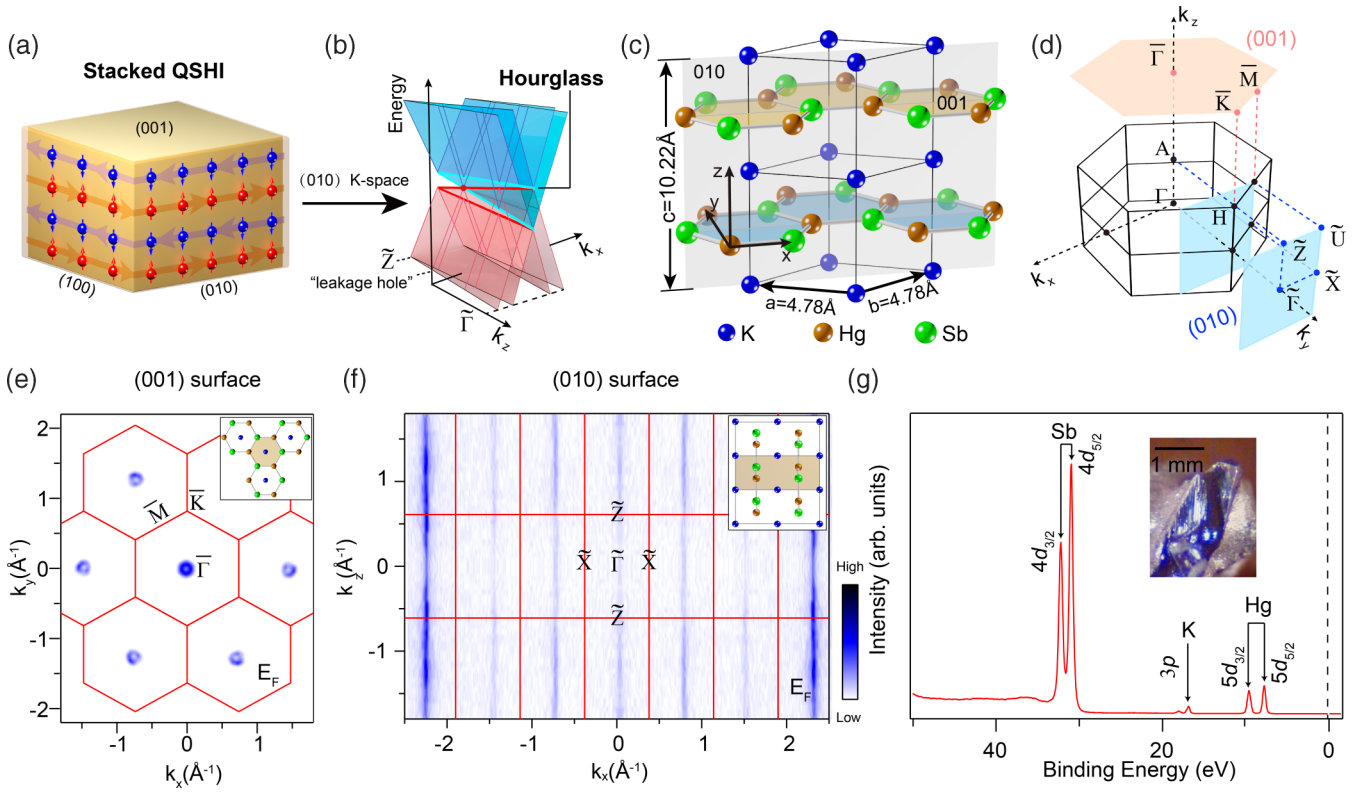

FIG. 1. Surface modes and basic characteristics of KHgSb. (a) Schematic showing the topological surface modes on the (100) and (010) surfaces of KHgSb. The four conducting branches of the surface mode on the (100) surface are almost dispersionless along k_z and play as a 3D counterpart of the 2D quantum spin Hall insulator, whereas those on the (010) surface delicately disperse along k_z, giving rise to the hourglasslike dispersion. (b) A schematic of the hourglasslike dispersion on the (010) surface. Slices along k_x indicate the evolution of the quadruplet surface states. (c) Crystal structure of KHgSb. Two of the possible cleaved surfaces, e.g., (001) and (010) surfaces, are highlighted with planes. A glide reflection exists on the (010) surface (gray). (d) Bulk and projected surface BZs of (001) and (010) surfaces; k_x, k_y, k_z are defined accordingly. (e) A large momentum scale of CEC at Fermi level taken by 90-eV linear horizontal polarized photons with an energy window of ±30 meV with respect to Fermi level on the (001) surface. Sixfold rotating symmetrization is applied with respect to $\bar{\Gamma}$. (f) A broad Fermi surface from (010) surface measured by 102-eV linear horizontal polarized photons with an energy window of ±30 meV with respect to Fermi level. Mirror symmetrization with respect to both $\tilde{X}$-$\tilde{\Gamma}$-$\tilde{X}$ and $\tilde{Z}$-$\tilde{\Gamma}$-$\tilde{Z}$ is employed. (g) The integrated photoemission spectra from core levels of KHgSb with Sb $4d_{3/2}$ and $4d_{5/2}$, K $3p$, Hg $5d_{3/2}$, and $5d_{5/2}$ captured.

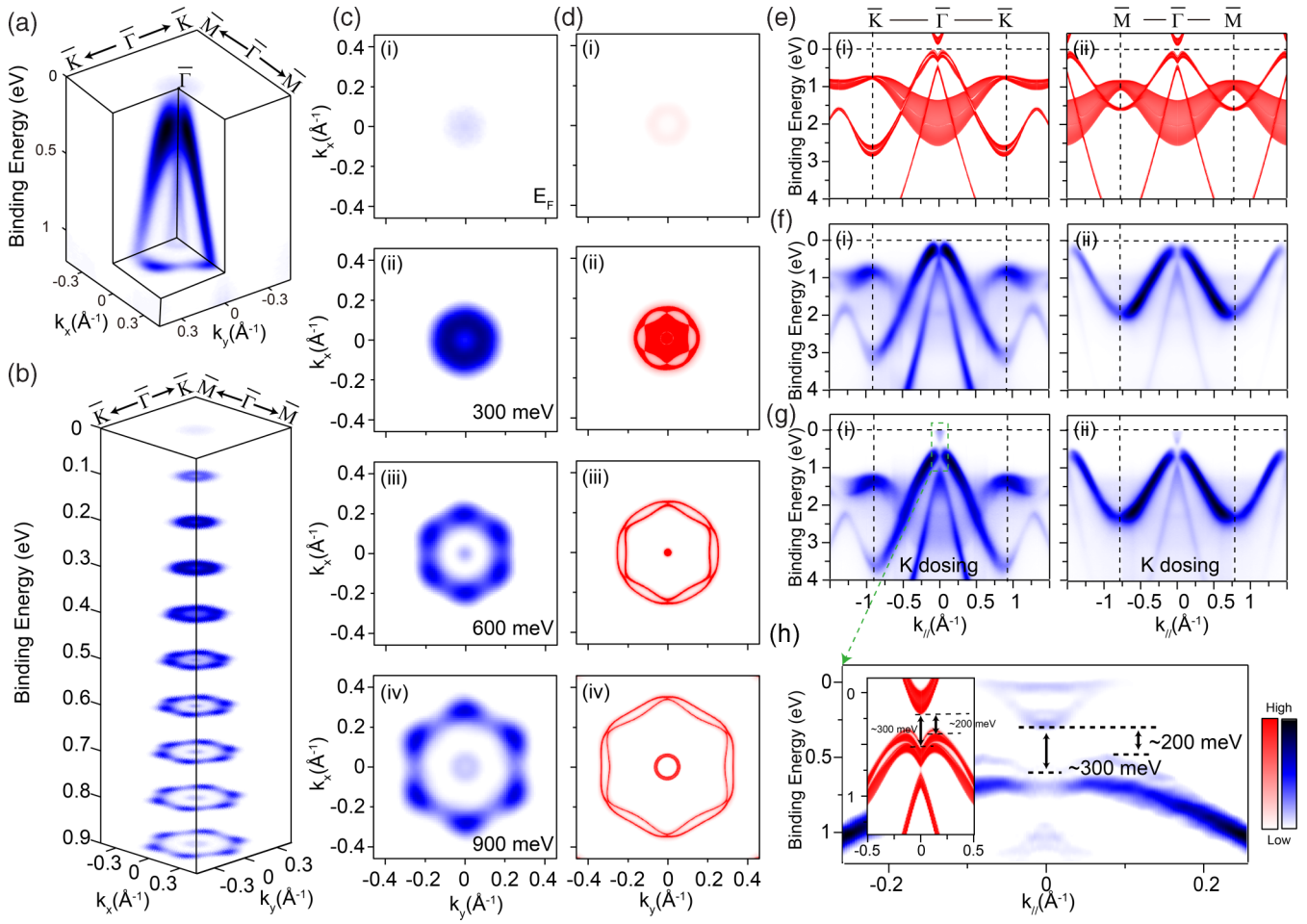

FIG. 2. Basic electronic structures on the (001) surface of KHgSb. (a) A 3D illustration of the in-plane electronic structure on the (001) surface of KHgSb. (b) Dense CECs near Fermi energy. (c) Selected CECs with binding energy $E_b = 0$ meV (i), 300 meV (ii), 600 meV (iii), and 900 meV (iv), respectively. (d) Calculated CECs corresponding to those in (c). (e) Calculated band structures along two high-symmetry directions, $\bar{K}$-$\bar{\Gamma}$-$\bar{K}$ (i) and $\bar{M}$-$\bar{\Gamma}$-$\bar{M}$ (ii), respectively. The indirect band gap of the conduction and valence band is ∼200 meV. (f) Extracted band dispersions along both $\bar{K}$-$\bar{\Gamma}$-$\bar{K}$ (i) and $\bar{M}$-$\bar{\Gamma}$-$\bar{M}$ (ii) directions. (g) The same band dispersions as those in (f) but with *in situ* potassium dosage to raise the Fermi energy. Full band gap is found without any signature of in-gap states in between the conduction and valence bands. (h) The zoomed-in band dispersion in (g) and (e). Second derivative method with respect to energy is employed. The experimental direct and indirect band gaps are noted. The data are measured with 80-eV photons with linear horizontal polarization. CECs in (a–c) are symmetrized by sixfold rotation with an integrated energy window of ±50 meV.

and dispersions along the high-symmetry directions $\bar{K}$-$\bar{\Gamma}$-$\bar{K}$ and $\bar{M}$-$\bar{\Gamma}$-$\bar{M}$ [Fig. 2(f)] show excellent agreement with the *ab initio* calculations [Figs. 2(d)–2(e), respectively].

In order to verify that there is no in-gap surface state residing in between the conduction and valence bands, we tuned the Fermi energy by introducing potassium (K) atoms *in situ* onto the sample surface so that the absorbed potassium atoms on the surface would donate free electrons. After K dosing, we could clearly observe the bottom of the conduction band and the top of the valence band simultaneously along both $\bar{K}$-$\bar{\Gamma}$-$\bar{K}$ and $\bar{M}$-$\bar{\Gamma}$-$\bar{M}$ directions [Fig. 2(g)]. An indirect band gap of ∼200 meV is observed with no signatures of in-gap surface states [Fig. 2(h)], agreeing with the calculations [Fig. 2(e)].

III. ELECTRONIC STRUCTURES ON THE (010) SURFACE

Next we demonstrate the detailed electronic structure on the (010) surface in Fig. 3. Figure 3(a) shows the stacked CECs. After inspecting CECs ranging from E_F to $E_b = 400$ meV [see Fig. 3(b) for experiments and Fig. 3(c) for *ab initio* calculations], one could observe that the CEC at E_F evolves gradually to high binding energies, until abruptly a different feature at the zone center with elliptical shape emerges at $E_b \sim 300$ meV [Figs. 3(b-iv) and 3(c-iv)]. The broad agreements between the experiments and *ab initio* calculations suggest the surface nature of the CECs near Fermi level [Figs. 3(b-i)–3(b-iii)] and the bulk origin of the elliptical shape pockets [Figs. 3(b-iv) and 3(b-v)], which can be further confirmed by the photon-energy-dependent ARPES measurements [Figs. 3(d) and 3(e)].

In Figs. 3(d) and 3(e), CECs taken in the k_x-k_y plane (i.e., taken along the $\tilde{X}$-$\tilde{\Gamma}$-$\tilde{X}$ direction by scanning photon energies) at $E_b = 0$ and $E_b = 400$ meV are plotted, respectively. The surface states form dispersionless straight lines along the k_y direction [Fig. 3(d)], showing no dependence on the photon energy and thus proving their surface origin. On the other hand,

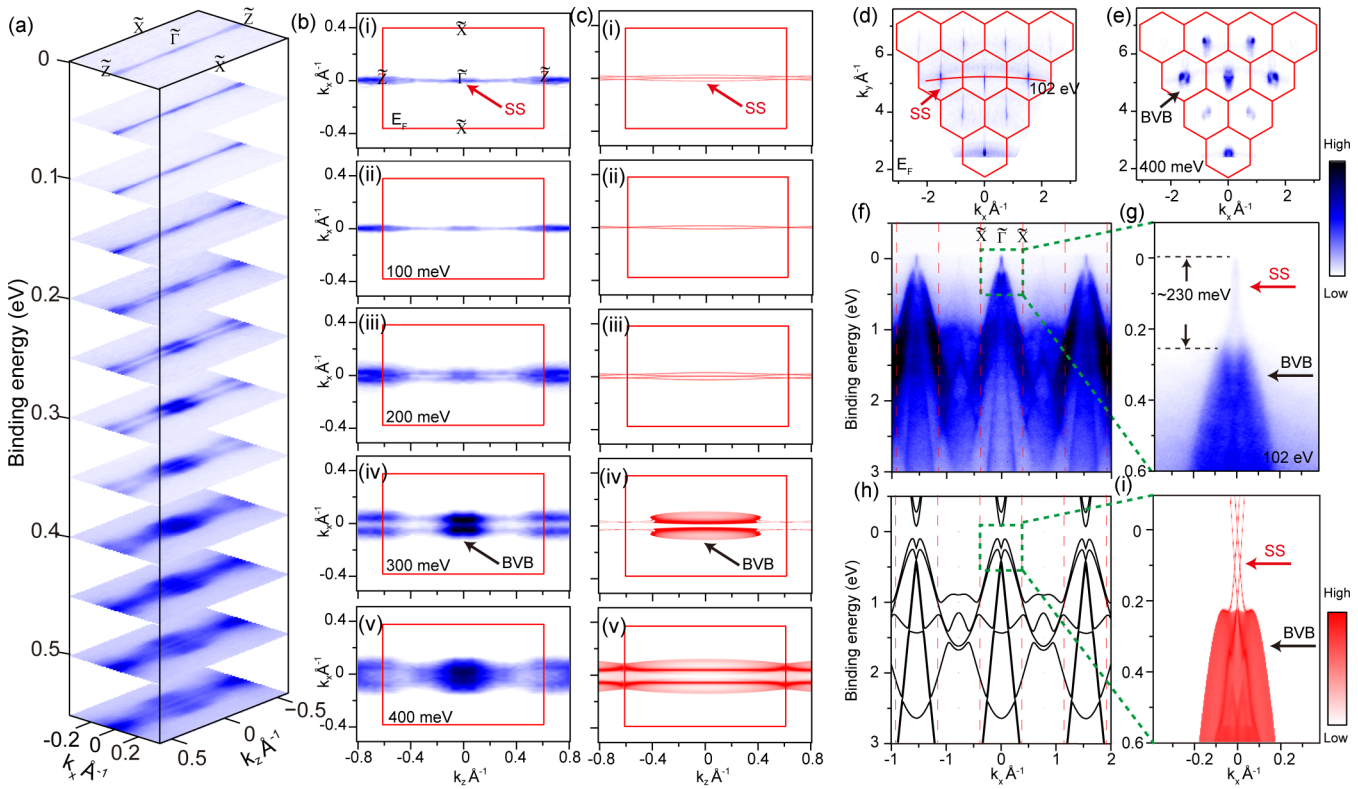

FIG. 3. Basic electronic structures on the (010) surface of KHgSb. (a) A slice illustration of the CECs on the (010) surface of KHgSb. (b) The selected CECs with binding energy $E_b = 0$ meV (i), 100 meV (ii), 200 meV (iii), 300 meV (iv), 400 meV (v). Spectra in (a,b) are measured with 102-eV photons with linear horizontal polarization. Data are mirror symmetrized with respect to the $\tilde{X}$-$\tilde{\Gamma}$-$\tilde{X}$ axis. (c) The calculated CECs (i–v) with energies in accordance to those in (b). The surface and the bulk parts of the contours are marked accordingly, BVB for bulk valence band and SS for surface state. (d,e) A large momentum space scale of Fermi surface and CEC at a binding energy of 400 meV in k_x-k_y momentum space by collecting photon-energy densely varied photoemission spectra along the $\tilde{X}$-$\tilde{\Gamma}$-$\tilde{X}$ direction. The one-dimensional-like dispersionless signatures in (d) indicate their surface nature and are thus marked as surface states, SS. The rounded hexagonal spots at each zone center of the (001) surface BZs in (e) imply their photon-energy variable sensitivity and thus are bulk states from the bulk valence band, marked as BVB. (f) The extracted cuts along $\tilde{X}$-$\tilde{\Gamma}$-$\tilde{X}$ taken by linearly horizontally polarized 102-eV photons with position denoted in (d). (g) The zoomed-in band dispersion in (f). (h) Calculated bulk bands along $\tilde{X}$-$\tilde{\Gamma}$-$\tilde{X}$ with $k_y = 0$. (i) Calculated zoomed-in projected band dispersion along $\tilde{X}$-$\tilde{\Gamma}$-$\tilde{X}$. All CECs are integrated by an energy window of ± 50 meV.

at $E_b = 400$ meV the surface states disappear and other bulk pockets emerge, showing strong k_y dispersion [Fig. 3(e)].

Finally, the electronic structures in Figs. 3(a), 3(c), and 3(e) can be well explained by the surface and bulk states shown in dispersions plotted in Figs. 3(f) and 3(g). While the surface states show a sharp linear dispersion [see features at $E_b = 0-230$ meV in Fig. 3(g)], the bulk states show typical broad dispersion extending to high binding energy [see features at $E_b > 230$ meV in Figs. 3(f) and 3(g)]. Again, the position and shape of both surface and bulk states are in good agreement with our *ab initio* calculations [see Fig. 3(h) for the bulk states only and Fig. 3(i) for both the bulk and surface states; more details can be found in SM.I of the Supplemental Material [70]].

In summary, our measurement on the (010) surface of KHgSb has demonstrated the gapped bulk states with an in-gap surface state, consistent with the *ab initio* calculations that predict KHgSb as a nonsymmorphic topological crystalline insulator [65].

IV. EVIDENCE OF HOURGLASSLIKE SURFACE FERMION

In order to confirm that KHgSb is a glide-reflection symmetry-protected topological crystalline insulator, we now focus on the details of the dispersion of the surface states on the (010) surface.

According to the calculation [65], the glide-reflection and time-reversal symmetry guarantee the emergence of the topologically robust hourglasslike surface fermion along the $\tilde{\Gamma}$-$\tilde{Z}$ direction [Fig. 1(b)] and the degeneracies of quadruplet surface states at $\tilde{\Gamma}$ and $\tilde{Z}$ [see the different slices parallel with k_x in Fig. 1(b)]. At $\tilde{\Gamma}$, the quadruplet surface states would form a characteristic rhombohedral-like shape close to the Fermi energy [see the first slice for schematic demonstration in Fig. 1(b) and calculation in Fig. 4(c-i)]. Between the two time-reversal invariant momenta at $\tilde{\Gamma}$ and $\tilde{Z}$, the degeneracies are lifted [see the second and third slices in Fig. 1(b) and calculation in Figs. 4(c-ii) and 4(c-iii)] and the two internal branches are switched, forming hourglasslike dispersion with

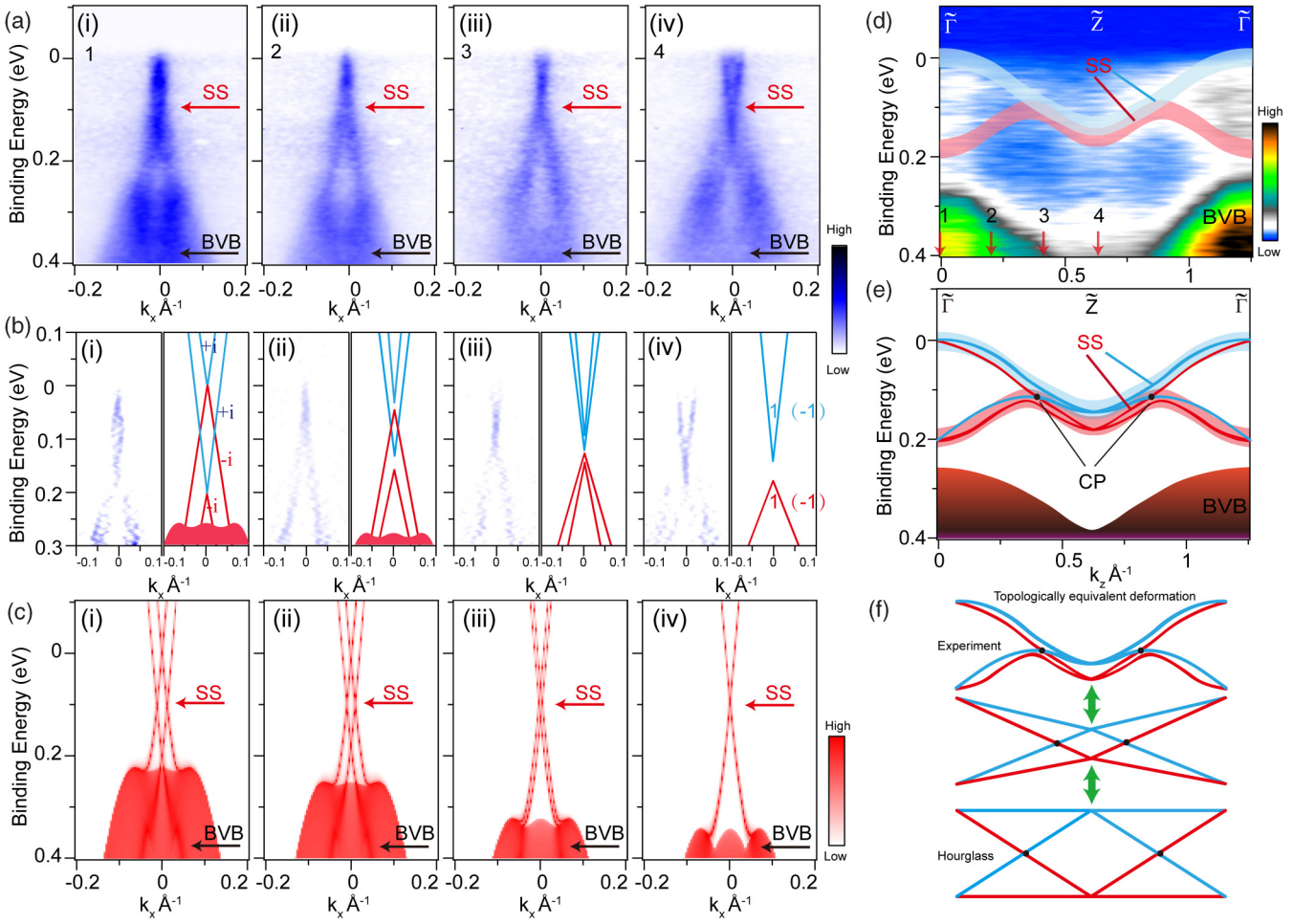

FIG. 4. The evidence of the hourglasslike surface fermion on the (010) surface of KHgSb. (a) The extracted band dispersions measured with 102-eV photons with linear horizontal polarization on the (010) surface which are parallel to the $\tilde{X}$-$\tilde{\Gamma}$-$\tilde{X}$ direction, covering half of the (010) surface BZ with $k_z \sim 0\,\text{Å}^{-1}$ (i), $0.2\,\text{Å}^{-1}$ (ii), $0.4\,\text{Å}^{-1}$ (iii), $0.6\,\text{Å}^{-1}$ (iv), respectively. The exact positions are noted in (d). The surface state and the bulk valence bands are also indicated by SS and BVB. (b) (i–iv) Each left panel is the second derivative image with respect to momentum corresponding to that in (a); each right panel schematically shows the evolution of the surface state, mimicking the behavior of each of the four surface-state branches. (c) Calculated band dispersions with similar momentum positions of band dispersions in (a). The surface-state branches and the bulk states are also labeled as SS and BVB. (d) The extracted band dispersion along the $\tilde{Z}$-$\tilde{\Gamma}$-$\tilde{Z}$ direction measured with 102-eV photons with linear horizontal polarization. The red and blue curves outline the trajectory of the surface state. (e) The most possible configuration of the four surface-state branches. The two internal branches intersect with each other and the total four surface-state branches give rise to a pair of distorted hourglass fermions along the $\tilde{Z}$-$\tilde{\Gamma}$-$\tilde{Z}$ direction. (f) The continuous deformation of the distorted dispersion of hourglass fermions in (e) to eventually show their topologically equivalence to the well defined hourglass configurations.

the crossing point [the "leakage hole" of the hourglass; see the third slice in Fig. 1(b)] at a certain momentum along $\tilde{\Gamma}$-$\tilde{Z}$. Further away from the crossing point, the two internal surface branches further separate, and eventually degenerate with their pseudo-Kramers counterparts at $\tilde{Z}$, and show a small gap between the upper and lower degenerate branches [see the fourth slice in Fig. 1(b) and calculation in Fig. 4(c-iv)].

In the ARPES measurements, we first investigate the evolution of the surface states' dispersions parallel to the $\tilde{X}$-$\tilde{\Gamma}$-$\tilde{X}$ direction at different k_z values, which are shown in Fig. 4(a) [with their k_z positions marked in Fig. 4(d), respectively]. To better visualize the details of the dispersions, the momentum second derivatives of the spectra intensity of dispersions are illustrated in Fig. 4(b) along with the schematics that show the surface-state dispersion evolutions.

Comparing the dispersions of the surface states [Figs. 4(a) and 4(b)] to those from *ab initio* calculations [Fig. 4(c)], we find that experimental results show considerable consistency with the calculation: Firstly, the most prominent feature in the number 1 cut [Figs. 4(a-i) and 4(b-i), $k_z = 0$ at $\tilde{\Gamma}$] is the rhombohedral shaped dispersion near the Fermi energy formed by the surface states. As discussed above, this feature is generated by the quadruplets containing two separate pairs of conjugated surface state branches [highlighted by the red and blue guidelines, Fig. 1(b-i)], each forming a Kramers degeneracy at $\tilde{\Gamma}$. Away from $\tilde{\Gamma}$ in the number 2 cut [Figs. 4(a-ii), 4(b-ii), $k_z = 0.2$ Å^{-1}, away from $\tilde{\Gamma}$],

the surface states change dramatically and the rhombohedral pattern shrinks, indicating the lift of the degeneracies. Moving further away from $\tilde{\Gamma}$ in the number 3 cut [Figs. 4(a-iii), 4(b-iii), $k_z = 0.4$ Å^{-1}], the two upper and the two bottom surface-state branches (pseudo-Kramers doublets) gradually disperse together. Thus in the number 3 cut, the rhombohedral feature disappears. Eventually, when the slice cuts across $\tilde{Z}$ in the number 4 cut [Figs. 4(a-iv) and 4(b-iv), $k_z = 0.6$ Å^{-1}], the pseudo-Kramers doublets become degenerate, as expected from a combined effect from both the time-reversal symmetry and the glide reflection. Even though the predicted small gap between the pseudo-Kramers doublets at $\tilde{Z}$ as well as the degeneracy of the two internal surface branches (hourglass leakage hole) are too small compared to the resolution of the ARPES measurements, the overall band dispersions and the evolution trend in experiment [Figs. 4(a) and 4(b)] basically agree with the calculation [Fig. 4(c)].

To reveal the hourglasslike dispersion of the quadruplet surface states, we extract their dispersion along the $\tilde{Z}$-$\tilde{\Gamma}$-$\tilde{Z}$ direction in Fig. 4(d). From the dispersion of the bulk valence band we could clearly identify the high-symmetry points $\tilde{\Gamma}$ and $\tilde{Z}$. The dispersion of the weak surface state is tracked and highlighted by the red and blue curves [Fig. 4(e)]. From the pattern of the dispersions [Figs. 4(b) and 4(d)] we could extract two (highly distorted) hourglass shapes from $\tilde{Z}$ to $\tilde{\Gamma}$ and $\tilde{\Gamma}$ to $\tilde{Z}$, which can evolve to a typical hourglass configuration [Fig. 4(f)] via continuous deformation (also see the movie clip in SM.II of the Supplemental Material [70]) and thus show their topological equivalence.

V. CONCLUSION

In summary, our ARPES measurements on KHgSb reveal its unique electronic structures on the (001) and (010) surfaces, and the agreement between experiments and the *ab initio* calculations on both surfaces strongly supports that KHgSb is a nonsymmorphic crystalline-symmetry-protected topological insulator, hosting a glide-reflection-protected topological hourglass fermion surface state on its side (010) surface. This discovery enriches the understanding of symmetry-protected topological quantum states and will open the door in searching unique topological quantum states and exotic fermions protected by other symmetries.

Note added. Comparing to a similar ARPES report on KHgSb recently [67], despite the general agreement on the observed electronic structures, we have noted the following differences. Firstly, the estimated bulk band gap size is ~200 (300) meV for the indirect (direct) ones [Fig. 2(h)] and ~460 meV in the previous report [67] [the calculated value is ~200 (300) meV for the indirect (direct) band gap, respectively; see inset of Fig. 2(h)]. Secondly, the band top of the bulk valence band along $\tilde{\Gamma}$-$\tilde{X}$ at $E_b \sim 230$ meV on the (010) surface seems to be absent in the previous report [67]. Thirdly, due to the mixture of the bulk continuum, we have not explicitly identified the four branches of the surface state at $E_b > 500$ meV on the (010) surface as reported in Ref. [67]. Instead, we take the rhombohedral feature formed at the surface-state crossings [Fig. 4(a-i)] as clear evidence of the surface-state quadruplet.

ACKNOWLEDGMENT

This work is supported by a grant from the National Key R&D program of China (2017YFA0305400) and Chinese Academy of Science—Shanghai Science Research Center, Grant No. CAS-SSRC-YH-2015-01. Y.L.C. acknowledges the support from the Engineering and Physical Sciences Research Council Platform Grant (Grant No. EP/M020517/1) and Hefei Science Center Chinese Academy of Sciences (2015HSC-UE013). Z.K.L. acknowledges the support from the National Natural Science Foundation of China (Grant No. 11674229). J.J. acknowledges the support of the National Research Foundation, Korea, through the SRC Center for Topological Matter (Grant No. 2011-0030787). C.C. acknowledges the support of the China Scholarship Council—University of Oxford Scholarship. H.F.Y. acknowledges financial support from the Bureau of Frontier Sciences and Education, Chinese Academy of Sciences. A.L.S. is supported by the U.S. DOE, Office of Basic Energy Sciences, under Contract No. DE-AC02-05CH11231. All authors contributed to the scientific planning and discussions. The authors declare no competing financial interest.

A.J.L. and J.J. contributed equally to this work.

APPENDIX: MATERIALS AND METHODS

1. Sample synthesis

K, Hg, and Sb were weighed in the atomic ratio 1:1:1 in an argon-filled glove box. Sb pieces were powdered and mixed with K and Hg and transferred to a quartz crucible. The crucible was put inside a quartz tube which was then evacuated and sealed. The tube was kept in a muffle furnace at 370 °C for 48 h. The temperature of the furnace was raised slowly (10 °C/h) to avoid sudden vaporization of K. The tube was broken inside the glove box and the contents were powdered and transferred to an alumina crucible and sealed inside a tantalum tube. The tantalum tube was put in a quartz tube, evacuated, and sealed. The contents were heated to 900 °C for 10 h and cooled down to 475 °C at a rate of 3 °C/h. The temperature was kept constant at 475 °C for 175 h and then rapidly cooled to room temperature. Shiny crystals of KHgSb were obtained which were stored inside a glove box.

2. Angle-resolved photoemission spectroscopy

Regular ARPES measurements were performed at the beamline I05 of the Diamond Light Source (DLS), BL 10.0.1, of the Advanced Light Source, both equipped with Scienta R4000 analyzers. The measured sample temperature and pressure were 10 K and lower than 1.5×10^{-10} Torr, respectively. The angle resolution was 0.2° and the overall energy resolutions were better than 15 meV. The air-sensitive KHgSb samples were first elaborately selected and prepared to realize two-surface cleavage in an Ar-filled glove box and they were cleaved *in situ* along the (001) and the (010) surfaces accordingly.

3. *Ab initio* calculations

The density-functional theory (DFT) calculations were performed by using the Vienna *ab initio* simulation package

(VASP) code with projector-augmented-wave (PAW) potential [71]. In order to get accurate band structures, we have used the modified Becke-Johnson exchange potential [72] for the exchange-correlation energy. For calculating the surface state, the tight-binding Hamiltonian matrix was constructed by projecting the bulk Bloch wave functions to the maximally localized Wannier functions (MLWFs) [73]. The surface state was calculated in the half-infinite boundary condition by using the iterative Green's function method based on the tight-model Hamiltonian [74].

[1] M. Z. Hasan and C. L. Kane, Rev. Mod. Phys. **82**, 3045 (2010).
[2] X.-L. Qi and S.-C. Zhang, Rev. Mod. Phys. **83**, 1057 (2011).
[3] C. L. Kane and E. J. Mele, Phys. Rev. Lett. **95**, 146802 (2005).
[4] B. A. Bernevig, T. L. Hughes, and S. C. Zhang, Science **314**, 1757 (2006).
[5] M. König, S. Wiedmann, C. Brüne, A. Roth, H. Buhmann, L. W. Molenkamp, X.-L. Qi, and S.-C. Zhang, Science **318**, 766 (2007).
[6] D. Hsieh, D. Qian, L. Wray, Y. Xia, Y. S. Hor, R. J. Cava, and M. Z. Hasan, Nature **452**, 970 (2008).
[7] H. Zhang, C.-X. Liu, X.-L. Qi, X. Dai, Z. Fang, and S.-C. Zhang, Nat. Phys. **5**, 438 (2009).
[8] Y. L. Chen, J. G. Analytis, J. H. Chu, Z. K. Liu, S. K. Mo, X. L. Qi, H. J. Zhang, D. H. Lu, X. Dai, Z. Fang, S. C. Zhang, I. R. Fisher, Z. Hussain, and Z. X. Shen, Science **325**, 178 (2009).
[9] L. Fu, Phys. Rev. Lett. **106**, 106802 (2011).
[10] T. H. Hsieh, H. Lin, J. Liu, W. Duan, A. Bansil, and L. Fu, Nat. Commun. **3**, 982 (2012).
[11] S. Y. Xu, C. Liu, N. Alidoust, M. Neupane, D. Qian, I. Belopolski, J. D. Denlinger, Y. J. Wang, H. Lin, L. A. Wray, G. Landolt, B. Slomski, J. H. Dil, A. Marcinkova, E. Morosan, Q. Gibson, R. Sankar, F. C. Chou, R. J. Cava, A. Bansil *et al.*, Nat. Commun. **3**, 1192 (2012).
[12] Y. Tanaka, Z. Ren, T. Sato, K. Nakayama, S. Souma, T. Takahashi, K. Segawa, and Y. Ando, Nat. Phys. **8**, 800 (2012).
[13] P. Dziawa, B. J. Kowalski, K. Dybko, R. Buczko, A. Szczerbakow, M. Szot, E. Łusakowska, T. Balasubramanian, B. M. Wojek, M. H. Berntsen, O. Tjernberg, and T. Story, Nat. Mater. **11**, 1023 (2012).
[14] Y. Tanaka, T. Sato, K. Nakayama, S. Souma, T. Takahashi, Z. Ren, M. Novak, K. Segawa, and Y. Ando, Phys. Rev. B **87**, 155105 (2013).
[15] Z. Wang, Y. Sun, X.-Q. Chen, C. Franchini, G. Xu, H. Weng, X. Dai, and Z. Fang, Phys. Rev. B **85**, 195320 (2012).
[16] Z. K. Liu, B. Zhou, Y. Zhang, Z. J. Wang, H. M. Weng, D. Prabhakaran, S. K. Mo, Z. X. Shen, Z. Fang, X. Dai, Z. Hussain, and Y. L. Chen, Science **343**, 864 (2014).
[17] S. Y. Xu, C. Liu, S. K. Kushwaha, R. Sankar, J. W. Krizan, I. Belopolski, M. Neupane, G. Bian, N. Alidoust, T. R. Chang, H. T. Jeng, C. Y. Huang, W. F. Tsai, H. Lin, P. P. Shibayev, F. C. Chou, R. J. Cava, and M. Z. Hasan, Science **347**, 294 (2015).
[18] A. Liang, C. Y. Chen, Z. J. Wang, Y. G. Shi, Y. Feng, H. M. Yi, Z. J. Xie, S. L. He, J. F. He, Y. Y. Peng, Y. Liu, D. F. Liu, C. Hu, L. Zhao, G. D. Liu, X. L. Dong, J. Zhang, M. Nakatake, H. Iwasawa, K. Shimada *et al.*, Chin. Phys. B **25**, 077101 (2016).
[19] Z. Wang, H. Weng, Q. Wu, X. Dai, and Z. Fang, Phys. Rev. B **88**, 125427 (2013).
[20] Z. K. Liu, J. Jiang, B. Zhou, Z. J. Wang, Y. Zhang, H. M. Weng, D. Prabhakaran, S. K. Mo, H. Peng, P. Dudin, T. Kim, M. Hoesch, Z. Fang, X. Dai, Z. X. Shen, D. L. Feng, Z. Hussain, and Y. L. Chen, Nat. Mater. **13**, 677 (2014).
[21] M. Neupane, S.-Y. Xu, R. Sankar, N. Alidoust, G. Bian, C. Liu, I. Belopolski, T.-R. Chang, H.-T. Jeng, H. Lin, A. Bansil, F. Chou, and M. Z. Hasan, Nat. Commun. **5**, 3786 (2014).
[22] S. Borisenko, Q. Gibson, D. Evtushinsky, V. Zabolotnyy, B. Buchner, and R. J. Cava, Phys. Rev. Lett. **113**, 027603 (2014).
[23] H. Yi, Z. Wang, C. Chen, Y. Shi, Y. Feng, A. Liang, Z. Xie, S. He, J. He, Y. Peng, X. Liu, Y. Liu, L. Zhao, G. Liu, X. Dong, J. Zhang, M. Nakatake, M. Arita, K. Shimada, H. Namatame *et al.*, Sci. Rep. **4**, 6106 (2014).
[24] J. Liu and D. Vanderbilt, Phys. Rev. B **90**, 155316 (2014).
[25] A. A. Burkov and L. Balents, Phys. Rev. Lett. **107**, 127205 (2011).
[26] H. Weng, C. Fang, Z. Fang, B. A. Bernevig, and X. Dai, Phys. Rev. X **5**, 011029 (2015).
[27] X. Wan, A. M. Turner, A. Vishwanath, and S. Y. Savrasov, Phys. Rev. B **83**, 205101 (2011).
[28] D. Bulmash, C.-X. Liu, and X.-L. Qi, Phys. Rev. B **89**, 081106 (2014).
[29] Z. K. Liu, L. X. Yang, Y. Sun, T. Zhang, H. Peng, H. F. Yang, C. Chen, Y. Zhang, Y. F. Guo, D. Prabhakaran, M. Schmidt, Z. Hussain, S. K. Mo, C. Felser, B. Yan, and Y. L. Chen, Nat. Mater. **15**, 27 (2016).
[30] B. Q. Lv, H. M. Weng, B. B. Fu, X. P. Wang, H. Miao, J. Ma, P. Richard, X. C. Huang, L. X. Zhao, G. F. Chen, Z. Fang, X. Dai, T. Qian, and H. Ding, Phys. Rev. X **5**, 031013 (2015).
[31] S. Y. Xu, N. Alidoust, I. Belopolski, Z. J. Yuan, G. Bian, T. R. Chang, H. Zheng, V. N. Strocov, D. S. Sanchez, G. Q. Chang, C. L. Zhang, D. X. Mou, Y. Wu, L. N. Huang, C. C. Lee, S. M. Huang, B. K. Wang, A. Bansil, H. T. Jeng, T. Neupert *et al.*, Nat. Phys. **11**, 748 (2015).
[32] L. X. Yang, Z. K. Liu, Y. Sun, H. Peng, H. F. Yang, T. Zhang, B. Zhou, Y. Zhang, Y. F. Guo, M. Rahn, D. Prabhakaran, Z. Hussain, S. K. Mo, C. Felser, B. Yan, and Y. L. Chen, Nat. Phys. **11**, 728 (2015).
[33] F. Y. Bruno, A. Tamai, Q. S. Wu, I. Cucchi, C. Barreteau, A. de la Torre, S. McKeown Walker, S. Riccò, Z. Wang, T. K. Kim, M. Hoesch, M. Shi, N. C. Plumb, E. Giannini, A. A. Soluyanov, and F. Baumberger, Phys. Rev. B **94**, 121112(R) (2016).
[34] Y. Wu, D. Mou, N. H. Jo, K. Sun, L. Huang, S. L. Bud'ko, P. C. Canfield, and A. Kaminski, Phys. Rev. B **94**, 121113 (2016).
[35] C. Wang, Y. Zhang, J. Huang, S. Nie, G. Liu, A. Liang, Y. Zhang, B. Shen, J. Liu, C. Hu, Y. Ding, D. Liu, Y. Hu, S. He, L. Zhao, L. Yu, J. Hu, J. Wei, Z. Mao, Y. Shi *et al.*, Phys. Rev. B **94**, 241119 (2016).
[36] L. Huang, T. M. McCormick, M. Ochi, Z. Zhao, M.-T. Suzuki, R. Arita, Y. Wu, D. Mou, H. Cao, J. Yan, N. Trivedi, and A. Kaminski, Nat. Mater. **15**, 1155 (2016).
[37] K. Deng, G. Wan, P. Deng, K. Zhang, S. Ding, E. Wang, M. Yan, H. Huang, H. Zhang, Z. Xu, J. Denlinger, A. Fedorov, H. Yang, W. Duan, H. Yao, Y. Wu, S. Fan, H. Zhang, X. Chen, and S. Zhou, Nat. Phys. **12**, 1105 (2016).

[38] J. Jiang, Z. K. Liu, Y. Sun, H. F. Yang, C. R. Rajamathi, Y. P. Qi, L. X. Yang, C. Chen, H. Peng, C. C. Hwang, S. Z. Sun, S. K. Mo, I. Vobornik, J. Fujii, S. S. Parkin, C. Felser, B. H. Yan, and Y. L. Chen, Nat. Commun. **8**, 13973 (2017).

[39] A. Tamai, Q. S. Wu, I. Cucchi, F. Y. Bruno, S. Riccò, T. K. Kim, M. Hoesch, C. Barreteau, E. Giannini, C. Besnard, A. A. Soluyanov, and F. Baumberger, Phys. Rev. X **6**, 031021 (2016).

[40] I. Belopolski, S.-Y. Xu, Y. Ishida, X. Pan, P. Yu, D. S. Sanchez, H. Zheng, M. Neupane, N. Alidoust, G. Chang, T.-R. Chang, Y. Wu, G. Bian, S.-M. Huang, C.-C. Lee, D. Mou, L. Huang, Y. Song, B. Wang, G. Wang *et al.*, Phys. Rev. B **94**, 085127 (2016).

[41] A. Liang, J. Huang, S. Nie, Y. Ding, Q. Gao, C. Hu, S. He, Y. Zhang, C. Wang, B. Shen, J. Liu, P. Ai, L. Yu, X. Sun, W. Zhao, S. Lv, D. Liu, C. Li, Y. Zhang, Y. Hu *et al.*, arXiv:1604.01706.

[42] N. Xu, Z. J. Wang, A. P. Weber, A. Magrez, P. Bugnon, H. Berger, C. E. Matt, J. Z. Ma, B. B. Fu, B. Q. Lv, N. C. Plumb, M. Radovic, E. Pomjakushina, K. Conder, T. Qian, J. H. Dil, J. Mesot, H. Ding, and M. Shi, arXiv:1604.02116.

[43] C. W. J. Beenakker, Annu. Rev. Condens. Matter Phys. **4**, 113 (2013).

[44] S. R. Elliott and M. Franz, Rev. Mod. Phys. **87**, 137 (2015).

[45] R. Yu, W. Zhang, H. J. Zhang, S. C. Zhang, X. Dai, and Z. Fang, Science **329**, 61 (2010).

[46] C. Z. Chang, J. S. Zhang, X. Feng, J. Shen, Z. C. Zhang, M. H. Guo, K. Li, Y. B. Ou, P. Wei, L. L. Wang, Z. Q. Ji, Y. Feng, S. H. Ji, X. Chen, J. F. Jia, X. Dai, Z. Fang, S. C. Zhang, K. He, Y. Y. Wang *et al.*, Science **340**, 167 (2013).

[47] M. N. Ali, J. Xiong, S. Flynn, J. Tao, Q. D. Gibson, L. M. Schoop, T. Liang, N. Haldolaarachchige, M. Hirschberger, N. P. Ong, and R. J. Cava, Nature **514**, 205 (2014).

[48] F. F. Tafti, Q. D. Gibson, S. K. Kushwaha, N. Haldolaarachchige, and R. J. Cava, Nat. Phys. **12**, 272 (2016).

[49] L. K. Zeng, R. Lou, D. S. Wu, Q. N. Xu, P. J. Guo, L. Y. Kong, Y. G. Zhong, J. Z. Ma, B. B. Fu, P. Richard, P. Wang, G. T. Liu, L. Lu, Y. B. Huang, C. Fang, S. S. Sun, Q. Wang, L. Wang, Y. G. Shi, H. M. Weng *et al.*, Phys. Rev. Lett. **117**, 127204 (2016).

[50] J. He, C. Zhang, N. J. Ghimire, T. Liang, C. Jia, J. Jiang, S. Tang, S. Chen, Y. He, S. K. Mo, C. C. Hwang, M. Hashimoto, D. H. Lu, B. Moritz, T. P. Devereaux, Y. L. Chen, J. F. Mitchell, and Z. X. Shen, Phys. Rev. Lett. **117**, 267201 (2016).

[51] J. Jiang *et al.* (unpublished).

[52] E. Mun, H. Ko, G. J. Miller, G. D. Samolyuk, S. L. Bud'ko, and P. C. Canfield, Phys. Rev. B **85**, 035135 (2012).

[53] Y. Wu, L.-L. Wang, E. Mun, D. D. Johnson, D. Mou, L. Huang, Y. Lee, S. L. Bud'ko, P. C. Canfield, and A. Kaminski, Nat. Phys. **12**, 667 (2016).

[54] A. Szilva, M. Costa, A. Bergman, L. Szunyogh, L. Nordström, and O. Eriksson, Phys. Rev. Lett. **111**, 127204 (2013).

[55] Y. Wu, T. Kong, L.-L. Wang, D. D. Johnson, D. Mou, L. Huang, B. Schrunk, S. L. Bud'ko, P. C. Canfield, and A. Kaminski, Phys. Rev. B **94**, 081108 (2016).

[56] X. H. Niu, D. F. Xu, Y. H. Bai, Q. Song, X. P. Shen, B. P. Xie, Z. Sun, Y. B. Huang, D. C. Peets, and D. L. Feng, Phys. Rev. B **94**, 165163 (2016).

[57] R. Lou, B. B. Fu, Q. N. Xu, P. J. Guo, L. Y. Kong, L. K. Zeng, J. Z. Ma, P. Richard, C. Fang, Y. B. Huang, S. S. Sun, Q. Wang, L. Wang, Y. G. Shi, H. C. Lei, K. Liu, H. M. Weng, T. Qian, H. Ding, and S. C. Wang, Phys. Rev. B **95**, 115140 (2017).

[58] S. A. Parameswaran, A. M. Turner, D. P. Arovas, and A. Vishwanath, Nat. Phys. **9**, 299 (2013).

[59] C.-X. Liu, R.-X. Zhang, and B. K. VanLeeuwen, Phys. Rev. B **90**, 085304 (2014).

[60] K. Shiozaki and M. Sato, Phys. Rev. B **90**, 165114 (2014).

[61] D. Varjas, F. de Juan, and Y.-M. Lu, Phys. Rev. B **92**, 195116 (2015).

[62] C. Fang and L. Fu, Phys. Rev. B **91**, 161105(R) (2015).

[63] K. Shiozaki, M. Sato, and K. Gomi, Phys. Rev. B **91**, 155120 (2015).

[64] X.-Y. Dong and C.-X. Liu, Phys. Rev. B **93**, 045429 (2016).

[65] Z. Wang, A. Alexandradinata, R. J. Cava, and B. A. Bernevig, Nature **532**, 189 (2016).

[66] A. Alexandradinata, Z. Wang, and B. A. Bernevig, Phys. Rev. X **6**, 021008 (2016).

[67] J.-Z. Ma, C.-J. Yi, B. Q. Lv, Z. J. Wang, S.-M. Nie, L. Wang, L.-Y. Kong, Y.-B. Huang, P. Richard, P. Zhang, K. Yaji, K. Kuroda, S. Shin, H.-M. Weng, B. A. Bernevig, Y.-G. Shi, T. Qian, and H. Ding, Sci. Adv. **3**, e1602415 (2017).

[68] M. Ezawa, Phys. Rev. B **94**, 155148 (2016).

[69] B. Yan, L. Muchler, and C. Felser, Phys. Rev. Lett. **109**, 116406 (2012).

[70] See Supplemental Material at http://link.aps.org/supplemental/10.1103/PhysRevB.96.165143 for details of photon-energy dependence of electronic structure on (010) surface (SM.I) and topological equivalence of the surface state on (010) surface and the hourglass configuration (SM.II).

[71] G. Kresse and J. Furthmuller, Phys. Rev. B **54**, 11169 (1996).

[72] F. Tran and P. Blaha, Phys. Rev. Lett. **102**, 226401 (2009).

[73] A. A. Mostofi, J. R. Yates, Y. S. Lee, I. Souza, D. Vanderbilt, and N. Marzari, Comput. Phys. Commun. **178**, 685 (2008).

[74] M. P. L. Sancho, J. M. L. Sancho, and J. Rubio, J. Phys. F: Met. Phys. **14**, 1205 (1984).